International Journal of Nanomedicine

Dovepress
open access to scientific and medical research

Open Access Full Text Article

ORIGINAL RESEARCH

Atomic Layer Deposition Coating of TiO_2 Nano-Thin Films on Magnesium-Zinc Alloys to Enhance Cytocompatibility for Bioresorbable Vascular Stents

This article was published in the following Dove Press journal:
International Journal of Nanomedicine

Fan Yang
Run Chang
Thomas J Webster

Department of Chemical Engineering, Northeastern University, Boston, MA 02115, USA

Background and purpose: A coronary stent is a well-known cardiovascular medical device implanted to resolve disorders of the circulatory system due to bloodstream narrowing. Since the implanted device interacts with surrounding biological environments, the surface properties of a typical implantable stent play a critical role in its success or failure. Endothelial cell adhesion and proliferation are fundamental criteria needed for the success of a medical device. Metallic coronary stents are commonly used as biomaterial platforms in cardiovascular implants. As a new generation of coronary stents, bioresorbable vascular scaffolds have attracted a great deal of attention among researchers and studies on bioresorbable materials (such as magnesium and zinc) remain a target for further optimization. However, additional surface modification is needed to control the biodegradation of the implant material while promoting biological reactions without the use of drug elution.

Methods: Herein, precise temperature and thickness controlled atomic layer deposition (ALD) was utilized to provide a unique and conformal nanoscale TiO_2 coating on a customized magnesium-zinc stent alloy.

Results: Impressively, results indicated that this TiO_2 nano-thin film coating stimulated coronary arterial endothelial cell adhesion and proliferation with additional features acting as a protective barrier. Data revealed that both surface morphology and surface hydrophilicity contributed to the success of the ALD nanoscale coating, which further acted as a protection layer inhibiting the release of harmful degradation products from the magnesium-zinc stent.

Conclusion: Overall, the outcome of this in vitro study provided a promising ALD stent coating with unique nano-structural surface properties for increased endothelialization, and as a result, ALD should be further studied for numerous biomedical applications.

Keywords: atomic layer deposition, titanium dioxide, magnesium, bioresorbable vascular scaffold, endothelium, cytocompatibility

Introduction

Heart arteries can be blocked or narrowed by a buildup of plaque which results in the reduction of blood flow to the heart and causes chest discomfort. In some cases, blood clots can suddenly form inside the artery to cause a complete block of the blood flow which leads to a heart attack. If coronary artery narrowing occurs, a stent may be required to reopen the blocked artery. Coronary stents are widely used in coronary artery heart disease treatments keeping arteries open to support

Correspondence: Thomas J Webster
Department of Chemical Engineering, Northeastern University, 313 Snell Engineering Center, 360 Huntington Avenue, Boston, MA 02115, USA
Tel +1 617 373 6585
Email th.webster@neu.edu

submit your manuscript | www.dovepress.com
DovePress
http://doi.org/10.2147/IJN.S199093

blood supply. The clinical surgery procedure is called Percutaneous Coronary Intervention (PCI) which requires a guideline to lead coronary stents to the place where plaque forms on the artery inner wall and coronary artery shrinkage occurs. Then, the coronary stents expand to compress the plaque to restore normal blood flow inside the coronary arteries. Coronary stents are now used in more than 90% of PCI procedures[1] and have evolved from balloon angioplasty to bare metal stents (BMS) then to drug-eluting stents (DES) and now to bioresorbable vascular scaffolds (BVS). The revolutionized treatment of coronary artery disease, balloon angioplasty, was initially without stent deployment.[2] With the clinical outcome of re-narrowing of coronary arteries due to acute vessel closure, bare metal stents were created to contemporarily support narrowed arteries. The first Food and Drug Administration (FDA) approved balloon-expandable slotted tube device, Palmaz-Schatz®, was invented by Johnson & Johnson.[3] The bare metal device was made of stainless steel and remained one of the most studied and widely used stents in the 1990s. However, BMS have high metallic density which resulted in a high risk of sub-acute stent thrombosis. Bare metal stents can prevent late luminal enlargement and induce vascular remodeling but can cause restenosis due to neointimal hyperplasia.[4] The technical challenges to implant BMS during the 1990s also resulted in frequent surgery failures of stent placement and embolization.[5] After upgrades for both surgical and stent device technologies, DES brought a new revolution to interventional cardiology. DES were BMS coated with anti-proliferative drugs such as sirolimus, paclitaxel, or everolimus which can substantially reduce the rate of in-stent restenosis compared with BMS.[6] However, an important side effect has emerged with drug-eluting stents that can be acute, subacute, and result in late stent thrombosis.

The implant region possesses endothelial damage, endothelial dysfunction, flow turbulence, and platelet dysfunction at least before reendothelialization has completed. The occurrence of thrombus inside the stent lumen is the result of platelet aggregation. Platelet adhesion takes place shortly after endothelial damage occurs. Through the process of platelet activation, a conformational change in the GP IIb/IIIa receptor, converting the receptor into a form that can bind fibrinogen and link with other platelets, results in platelet aggregation. Inflammation and especially hypersensitivity inflammation play an essential role in stent thrombosis.[7]

Hypersensitivity-associated Kounis syndrome is a major issue related to hypersensitivity inflammation. Kounis syndrome has been defined as the concurrence of chest pain, chest discomfort, coronary spasm, myocardial infarction, stent thrombosis, hypotension, dyspnea, vomiting, syncope, urticaria, bradycardia, etc.[8] Kounis syndrome is associated with mast cell and platelet activation interacting with inflammatory cells, such as macrophages and T-lymphocytes. Therefore, new research should be focused on the pathophysiology of stent thrombosis and discovering short-term scaffolds and non-allergenic materials to avoid hypersensitivity inflammation and stent thrombosis.[9]

Currently, permanent metal and polymer scaffolds are implanted into coronary arteries to function as a long-term (>1 year) vascular stent. However, chronic or long-term clinical issues may occur due to the toxicity of implant materials since these materials cannot be safely absorbed by the human body. For example, contemporary metallic drug-eluting stents have great clinical outcomes within 1 year of implantation. After 1 year, however, stent-related adverse events may appear such as thrombosis, restenosis, and even myocardial infarction from blocked arteries. Additionally, chronic inflammation, neoatherosclerosis, and strut fracture may affect the whole human body. Further surgery may be required to remove the stent placing a risk for plaque buildup which would require more stents to be placed in the artery.[6] BVS is an alternative solution especially designed for stent implantation as the scaffold can be fully absorbed by the human body safely without the need for secondary surgeries to remove permanent stents, subjecting the patient to a reduced risk of further chronic diseases. Biodegradable stents combine the bioresorbable-bioabsorbable stent technology that has been developed to reduce or to eliminate late stent thrombotic risks. With bioresorbable technology, all stent components (drugs and/or scaffolds) are fully absorbed and leave nothing behind inside the human body, while with bioabsorbable stents, only the drug is absorbed which leaves a bare metal scaffold behind.[6]

The complete life cycle of BVS includes three phases: revascularization, restoration, and resorption. Revascularization involves alleviating coronary stenosis ischemia-production which is similar to DES when drug elution occurs within the first 5–6 months. Restoration is when the scaffold starts to experience mass loss followed by a reduction in molecular weight after 6 months of implantation. Finally, depending on the degradation rate of the stent, the resorption process can take up to 2–4

years. Recovery of the vascular structure and function occurs within the revascularization process. After the BVS has finished its functionality to remodel the coronary artery, it starts to disappear throughout the next two phases of the BVS life cycle. The FDA has approved only one BVS invented by Abbott[10] with poly (lactic acid) (PLLA) as the stent platform. This BVS has been reported to show positive vessel remodeling and plaque regression during the resorption process between 1 and 5 years after implantation.[11,12] However, polymeric stents in general have a lower tensile strength, reduced stiffness, and reduced ductility compared to metallic stents. Also, polymeric DES have been reported to have late thrombosis clinical issues.[6]

Reports have demonstrated that bioresorbable scaffold components can induce local foreign body reactions and hypersensitivity reactions. Upon stent implantation, several proteins (such as albumin, fibronectin, and fibrinogen) adsorb on the surface of the implant. The implant, as a foreign substance, is recognized by macrophages due to protein adsorption on the surface, and the presence of such implanted scaffolds results in macrophage differentiation and transformation into foreign body giant cells.[13] In the case of polymer scaffolds, during poly-L-lactic-acid (L-lactic-co-glycolic acid) degradation, acidic degradation products (such as lactic and glycolic acid) decrease the pH of the surrounding tissues which can trigger inflammatory and foreign body reactions in vivo.[14,15] Reports have also shown that poly(D,L-lactic-co-glycolic) acid polymer scaffolds may cause stent thrombosis. Biocompatibility issues regarding poly(D,L-lactic-co-glycolic) acid degradation products after implantation have made this polymer material no longer biologically inert.[16] Even though the FDA approved the Absorb GT1™ Bioresorbable Vascular Scaffold (BVS) System-P150023 in 2016, the following suggestions were made: Absorb GT1 BVS is contraindicated for patients who have a known hypersensitivity or allergy to everolimus, materials used in the device (such as poly(L-lactide) and poly (D,L-lactide)) contrast media, aspirin, antiplatelet agents or platinum.[17] On the other hand, metallic biomaterials are very popular for biomedical applications since for the most part such hypersensitive or allergic reactions have not been documented (for example, for magnesium).

There is enormous interest for magnesium (Mg) alloys among researchers for industrial and biomedical applications because of its great mechanical properties, biocompatibility, and biological resorbability. Magnesium ions in these alloys participate in many metabolic reactions and biological mechanisms. The large number of magnesium ions present naturally in the human body highlight their biocompatibility. Normally, the human body contains approximately 35 g of Mg per 70 kg of body weight and the daily intake of Mg is 375 mg.[18] The key feature of Mg for biomedical applications is that it is biodegradable. This feature may be very important when considering Mg as a platform for a BVS. Magnesium alloys have advantages over traditional ceramics, biodegradable polymers, and other metallic materials. With its excellent mechanical properties of lightweight, high mechanical strength, and high fracture toughness, many types of Mg stents have been developed by many companies since 2004.

For example, Biotronik introduced three generations of absorbable metal stents (AMS) with the WE43 magnesium alloy as the platform. The first clinical study showed a safe AMS inserted into the coronary arteries of 63 patients for 4 months. A third generation of AMS was coated with a degradable polymer carrier with an antiproliferative drug and showed positive results of safety and efficacy compared to previous AMS during in vivo trials.[19] However, WE43 still contains 4% yttrium and 2.25% rare earth metals which may be considered to be toxic or hepatotoxic to humans. In order to develop new generations of BVS, new materials should be used which are non-toxic (or at least have low toxicity).

In this article, a magnesium-zinc (Mg-Zn) binary alloy was coated with a nano-film of TiO_2 as a potential new platform for BVS. Zinc (Zn), as one of the most abundant nutritionally essential elements in the human body, exists in all human tissues.[20] Aside from the physiologically essential need of Zn, Zn also exhibits strong anti-atherogenic properties.[21] Furthermore, Zn has been used to improve the mechanical properties of Mg for commercial applications. It has been reported that the viscera histology examination and biochemical measurements proved the degradation products of Mg-Zn would not damage major organs and the Mg-Zn alloy has good biocompatibility during in vitro cytotoxicity tests with an L929 cell line.[22,23] Nevertheless, the downside of a Mg-Zn binary alloy is critical with a high corrosion rate that produces H_2 gas in vitro and in vivo.[19] In order to slow down the initial corrosion rate of a Mg-Zn alloy, surface modifications with coating technologies are recommended. To allow the implants to biodegrade and be absorbed by the human body completely, the coatings should act as a corrosion barrier to cease corrosion at different stages.[24]

Ideally, the coatings should also degrade gradually in order to control the overall corrosion rate of the implant device and leave no harm to the human body throughout the entire process. Possible coating technologies for biomaterials include metal-metal coatings, chemical vapor deposition (CVD), ion beam assisted deposition (IBAD), atomic layer deposition (ALD), pulsed laser deposition (PLD), etc. Coating technologies such as IBAD and PLD will require a line of sight for deposition which is limited for complex shapes.[25,26] On the other hand, atomic layer deposition (ALD) provides a uniform, chemically bonded, pinhole-free and controlled thickness coating on individual primary surfaces. Since ALD is independent of line of sight, internal structures can also be coated conformally. Even though CVD, and similarly ALD, can also deposit a chemically bonded coating with vapor deposition, ALD has the unique ability to split binary reactions into two self-limiting half-reactions that occur on the substrate surface.[27] Besides, ALD reactions are self-terminating with precise thickness controlled by deposition cycles and with good reproducibility applicable to sensitive substrates, such as biomaterials.[28]

In this study, ALD was chosen to deposit a biologically inspired nanoscale thin film coating on structural Mg-Zn binary alloys. Tetrakis(dimethylamido)titanium (TDMATi) was chosen as the ALD precursor to deposit titanium dioxide (TiO_2) on the alloys. Nano-sized TiO_2 is used widely in a variety of daily products, such as antifouling paints, plastic goods, sunscreens, pharmaceutical additive agents and food colorants.[29] The FDA claims that TiO_2 may be safely used as a color additive for coloring food products in quantities up to 1% by weight.[30] TiO_2 is also used in oral pharmaceutical formulations and the pharmaceutical excipients handbook considers nano-sized TiO_2 as a non-toxic excipient (which is, of course, dependent on concentration).[31] Since TiO_2 has also shown good corrosion resistance on steel surfaces using the sol-gel method, it can become a protective barrier for the Mg-Zn substrates.[32] An ALD coating of TiO_2 was previously used for a 316LVM steel base for vascular stents with coating temperatures modified in order to compare the mechanical properties of different samples. The results showed an increase in temperature and had an adverse effect on corrosion resistance and a temperature above 300°C will significantly decrease material hardness.[33] Thus, for this study, coating temperatures were chosen to deposit TiO_2 at 150°C and 200°C. Both TDMATi and H_2O were purged into the reaction chamber in order to chemically bond TiO_2 to the substrate (Mg-Zn). Biocompatibility experiments and surface morphology characterization studies were conducted for the Mg-Zn alloys coated with TiO_2 by ALD and control samples of Mg-Zn alloys without ALD treatments.

Materials and Methods

TiO_2-Coated Sample Preparation

Magnesium alloy (ZK61M) plates (1 mm thickness) were customized to only include Mg and Zn without any impurities. Samples were purchased from Kaiqi Mold Steel Ltd., Dongguan, China. The ALD instrument was donated by Ultratech, Inc. (Waltham, MA). Mg-Zn alloy samples were cut into identical pieces (0.5 inch × 0.5 inch). Samples were cleaned with 100% isopropyl alcohol (IPA) and 70% ethanol for 20 mins, respectively. Then, the samples were dried at 100°C inside an oven for 10 mins. The cleaned samples were placed into a preheated ALD chamber. A vacuum pump was used to create a vacuum inside the reaction chamber. Titanium dioxide (TiO_2) thin films were deposited onto the Mg-Zn substrates using TDMATi and H_2O as ALD precursors. Nitrogen gas served as a purging gas fed to the chamber during the entire coating process.[34] In this study, a single standard ALD cycle consisted of a 0.1 s exposure to TDMATi, 10 s of N_2 purge, 0.015 s exposure to H_2O, and again 10 s of N_2 purge, repeatedly. The total flow rate of the N_2 gas was 100 standard cubic centimeters per minute (sccm). The TiO_2 thin films were deposited at two different temperatures, 150°C and 200°C. For 100 nm of the TiO_2 coatings to be applied on the Mg-Zn alloys, 2500 cycles were used to complete the recipe since 0.4 Å was coated per cycle.

Surface Characterization

The surface morphology of the samples was characterized by scanning electron microscopy (SEM, Hitachi S-4800). The qualitative and quantitative analysis of titanium scans for samples soaked in medium for 0 and 3 days was conducted using X-ray Photoelectron Spectroscopy (XPS, XRA008 Thermo Scientific K-alpha plus XPS System) with the data analysis software Avantage. Compositional analysis was conducted using Energy-dispersive X-ray Spectroscopy (EDAX, Hitachi S-4800). An Atomic Force Microscope (AFM; Parks Scientific XE-7 AFM) was used to measure surface roughness of the ALD-treated Mg-Zn samples. Each sample was analyzed under non-contact mode using a silicone ultrasharp cantilever (MikroMasch). A 2 μm × 2 μm AFM field was analyzed for each sample

and the scan rate was chosen to be 0.5 Hz. Image analysis software (XEI) was used to generate 3D topography images and to compare the root-mean-square (RMS) roughness of the samples obtained by the software. The crystallinity of the TiO_2 layers was investigated using an X-ray Diffractometer (XRD, Ultima, Rigaku Corp.) fitted with Cu Kα radiation. The XRD was operated at 40 kV and 44 mA with a step width of 0.1θ and a count time of 0.5 s. The scanning range (2θ) of the XRD trial was 20–90°. Phase identification was performed using the standard JCPDS database. To assess the sample surface wettability, water contact angles were measured using a ProScope HR Microscope at room temperature. A droplet of deionized water was added to each sample surface. Three identical samples were measured to calculate contact angle results. The average contact angle was determined, and the Owens–Wendt method[35] was used to calculate the surface free energy:

$$\gamma_s^d = \frac{\gamma_l^d(1+cos\theta)^2}{4}; \quad \gamma_l^t(1+\cos\theta) = 2\left(\sqrt{\gamma_l^p\gamma_s^p} + \sqrt{\gamma_l^d\gamma_s^d}\right); \quad \gamma_s^t = \gamma_s^d + \gamma_s^p$$

Here, γ_s^d, γ_s^p, and γ_s^t are the dispersive, polar, and total components of the substrate surface energy; γ_l^d, γ_l^p, and γ_l^t are dispersive, polar, and total components of the liquid surface tension, respectively; and θ is the contact angle as determined.

Protein Adsorption Assays

A bicinchoninic acid (BCA) protein assay kit (Thermo Scientific) was used to quantify the total amount of bovine serum albumin (BSA) adsorbed onto the sample surfaces. 1 mg/mL (0.1%) of a BSA solution was prepared by diluting 30% BSA with PBS. Each sample was treated with 1 mL of a 0.1% BSA solution and cultured for 24 hrs in an incubator (37°C, humidified, 5% CO_2). After that, the BSA solution was aspirated and each sample was washed with 1 mL of PBS to remove non-adsorbed proteins. Then, each sample was treated with 1 mL of RIPA buffer (Sigma-Aldrich) for 10 mins to solubilize the adsorbed proteins. A working reagent (WR) was prepared using a BCA protein assay kit with a 50:1 ratio of Reagent A:B. According to the BCA assay microplate protocol, the desired amount of the BSA final concentration was mixed with the corresponding WR and put into a dry bath at 37°C. Finally, 200 µL of each BSA sample was transferred to a 96-well tissue culture plate and tested at a wavelength of 562 nm by a plate reader (Molecular Devices, SpectraMax M3).

Cell Assays

Cell Culture

Human Coronary Artery Endothelial Cells (HCAECs, PromoCell, C-12221) were used for all mammalian cell experiments. Primary endothelial cells were cultured in Endothelial Cell Growth Medium (PromoCell, C-22010) with an endothelial cell growth medium supplemental mix (PromoCell, C-39215) added to the growth medium. An additional 5 mL of a 1% penicillin/streptomycin (P/S; Sigma-Aldrich) solution was added to the Endothelial Cell Growth Medium and filtered and stored in a 4°C fridge. All cells were incubated in a 37°C, humidified, 5% CO_2 and 95% air environment.

Fluorescent Microscopy Imaging

Cells were allowed to attach to the samples at a seeding density of 100,000 cells per well. After 4 hrs of incubation, the samples were washed three times with PBS and then stained for fluorescence microscopy analysis. A 3.7% formaldehyde solution was used to fix the cells on the samples. The samples were further permeabilized with 0.1% Triton X-100 solution for 5 mins. Rhodamine and Hoechst (Life Technologies) actin stain dyes were used to stain the adherent cells on each sample. Finally, the samples were turned upside down in a new 12-well plate and imaged using a Zeiss Axio Observer Z1 with Zen 2 Pro Software.

Cell Adhesion and Proliferation Assays

To determine the proliferation of HCAECs on the Mg-Zn alloy, samples were placed individually into 12-well non-tissue culture plates and sterilized with UV light inside a biohazard hood for 1 hr. 1 mL of cell medium was added to each well and incubated for 1 hr. Cells were seeded onto each sample at a density of 10,000 cells/cm^2. For cell adhesion, endothelial cells were incubated for 4 hrs at a 37°C, humidified 5% CO_2 atmosphere. Cell proliferation was measured at 7 days and 14 days of culture. Cell growth medium was changed every 2 days during the proliferation period. Phosphate buffered saline (PBS) was used to wash off dead cells and 1 mL of PBS was added to each sample and aspirated before adding new growth medium. After incubation, each sample was washed with 1 mL PBS and an MTS dye (Promega) solution at a 1:5 ratio (MTS: Medium) was prepared. Each sample was carefully transferred to a new

12-well tissue culture plate with a 1.2 mL MTS solution added into each well. Next, 12-well tissue culture plates were covered with aluminum foil and cultured for another 4 hrs to allow for the complete reaction of the MTS dye with the metabolic products of the adherent cells. Then, 100 µL of the reacted solution from each well was transferred to a 96-well tissue culture plate in triplicate. Finally, cell density data were determined from the absorbance measured by a plate reader (Molecular Devices, SpectraMax M3) at a wavelength of 490 nm.

Statistics

All cell studies were conducted in triplicate and repeated at least three times. Data were collected and the significant differences were assessed with the probability associated with ANOVA followed by Student's *t*-tests, only compared to control data. Statistical significance was considered at a p-value of less than 0.05.

Results

Surface Characterization

ALD can be applied to many surfaces to allow for titanium dioxide (TiO_2) thin film growth on top of flat or rough surfaces. It has been reported that crystal structures can appear when TiO_2 film growth temperatures reach above 165°C.[36] The surface morphology of the Mg-Zn alloy control and ALD-treated Mg-Zn alloy (150°C and 200°C) was visualized by SEM (Figure 1A–C). It was clearly shown that TiO_2 thin films coated by ALD onto Mg-Zn alloy surfaces remarkably changed surface structures. Agglomeration appeared intensively with an increase in temperature from 150°C to 200°C. Crystallites formed on the thin film surfaces were observed at an ALD temperature at 200°C.

AFM was performed to visualize surface topography and measure the surface roughness of each sample. The RMS roughness results showed an increase of surface roughness from 12.05 nm (Mg-Zn control) to 34.77 nm

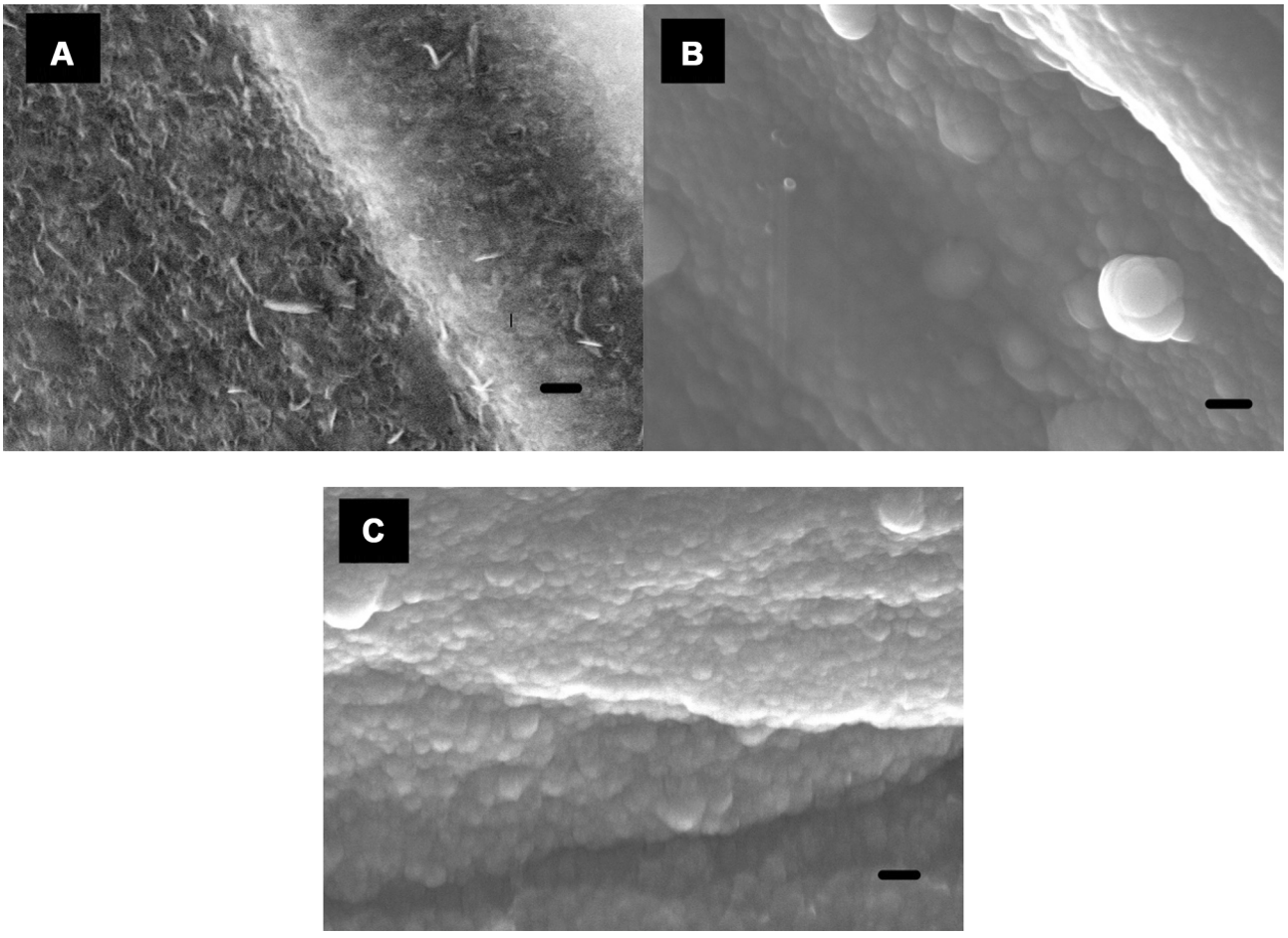

Figure 1 Scanning electron microscopy images of (**A**) Mg-Zn control, (**B**) Mg-Zn-TiO_2 (150°C), and (**C**) Mg-Zn-TiO_2 (200°C); scale bars are 200nm.
Abbreviations: Mg, magnesium; Zn, zinc; TiO_2, titanium dioxide.

(Mg-Zn-TiO_2-150°C). However, TiO_2 coated at 200°C did not change surface roughness (12.23 nm, Figure 2).

The elemental concentration of each SEM tested sample was determined by EDAX as shown in Figures 3–5. In Table 1, the elemental weight percentages and atomic percentages of TiO_2 coated samples are summarized compared with the Mg-Zn alloy control. The notable increase of titanium (Ti) and oxygen (O_2) indicated the existence of TiO_2 films deposited on the substrate surface.

XPS graphs with titanium scans also showed the existence of TiO_2 with two peaks at 465 eV and 459 eV (Figure 6A). After 3 days of soaking in cell medium (Figure 6B), the TiO_2 thin film layer disappeared since only one peak was presented for the sample with a 200°C ALD coating. TiO_2 coated at 150°C still presented two peaks (Figure 6B) indicating the maintenance of a TiO_2 thin film.

The XRD patterns of the tested samples are shown in Figure 7. X-ray diffraction peaks were observed to fit with standard JCPDS data and compared with similar Mg-Zn alloy patterns.[37] A diffraction peak at 2θ=25.7° for Mg-Zn-TiO_2 (200°C) indicated the formation of TiO_2 crystalline anatase as compared with Mg-Zn-TiO_2 (150°C) and the control.

Surface wettability, which is determined by surface topography and chemistry, can further affect protein adsorption and, thus, cell attachment, on the substrate and therefore is one of the key factors for investigating cell activities on an implant.[38,39] The surface wettability of the Mg-Zn alloy control and Mg-Zn-TiO_2 (150°C and 200°C) was determined from static water contact angle measurements. Hydrophobicity and hydrophilicity were determined by comparing contact angles result between samples. In Figure 8, TiO_2 coatings on Mg-Zn alloy substrates were found to be slightly more hydrophobic than controls. Mg-Zn alloy controls were more hydrophilic with contact angles around 44.5°. TiO_2 coated at 150°C showed a slight increase of contact angle (52.5°) compared to the control. The contact angle for the 200°C thin film coatings increased to 65° indicating that the sample was much more hydrophobic than the Mg-Zn control and those prepared at 150°C. By averaging three contact angle results, surface energy was calculated based on the Owens–Wendt method (Table 2). The dispersive surface energy is related to van der Waals and other non-site specified interactions. The polar surface energy is associated with dipole-dipole, hydrogen bonding, and other site specified interactions. As shown in Table 2, the total surface energies were relatively lower for the Mg-Zn alloys coated with TiO_2 compared to the Mg-Zn control surface.

Protein Adsorption Effect

According to the results obtained from the BCA protein adsorption assay (Figure 9), the ALD-coated Mg-Zn alloy samples slightly increased protein adsorption (but not statistically) when compared with the Mg-Zn control after soaking in a 0.01% BSA protein solution for 24 hrs. However, the level of protein adsorption on ALD-treated samples showed no statistical significance compared to the untreated control.

Fluorescent Microscopy Assays

Fluorescent microscopy experiments employing Rhodamine/Hoechst (red/blue signals) dyes were carried out. Fluorescent micrographs of HCAECs cultured for 4 hrs on the Mg-Zn control and Mg-Zn-TiO_2 (150°C and 200°C) samples showed that HCAECs initially adhered on the Mg-Zn alloy surfaces. Control samples clearly showed cell adhesion on Mg-Zn with blue signals indicating cell nuclei stained by Rhodamine. Red signals represent cell membranes stained by Hoechst dye. As shown in Figure 10A, without ALD coatings, HCAECs only adhered to sample surfaces but did not promote cell spreading as the attached cells displayed limited spreading and F-actin composition as indicated by the red fluorescence. Samples with the TiO_2 coated at 150°C showed impressive cell spreading (Figure 10B) as a majority of the cells had greater cytoskeleton staining. On the other hand, samples coated at 200°C did not show significantly enhanced cell spreading as compared to the 150°C samples (Figure 10C).

Cell Assays

HCAECs form an important cell monolayer that lines blood vessels, maintains vascular tone, regulates hemostasis, protects blood vessel from toxic matters, and controls inflammation.[40] During PCI, expanding of the coronary stent might cause damage to the monolayer of HCAECs that lines the blood vessel. Therefore, a successful coronary scaffold should have the ability to promote the growth of HCAECs in order to heal and reconstruct the blood vessel. In other words, a promising implantable material should accelerate HCAECs growth and protect the blood vessel from inflammation, and balance thrombosis and clotting. Thus, the effect of the nanoscale TiO_2 thin film coatings by ALD on HCAECs cell proliferation was investigated for Mg-Zn-TiO_2 (150°C and 200°C) and Mg-Zn control samples. As a result, after 7 and 14 days of cell culture, the endothelial cell

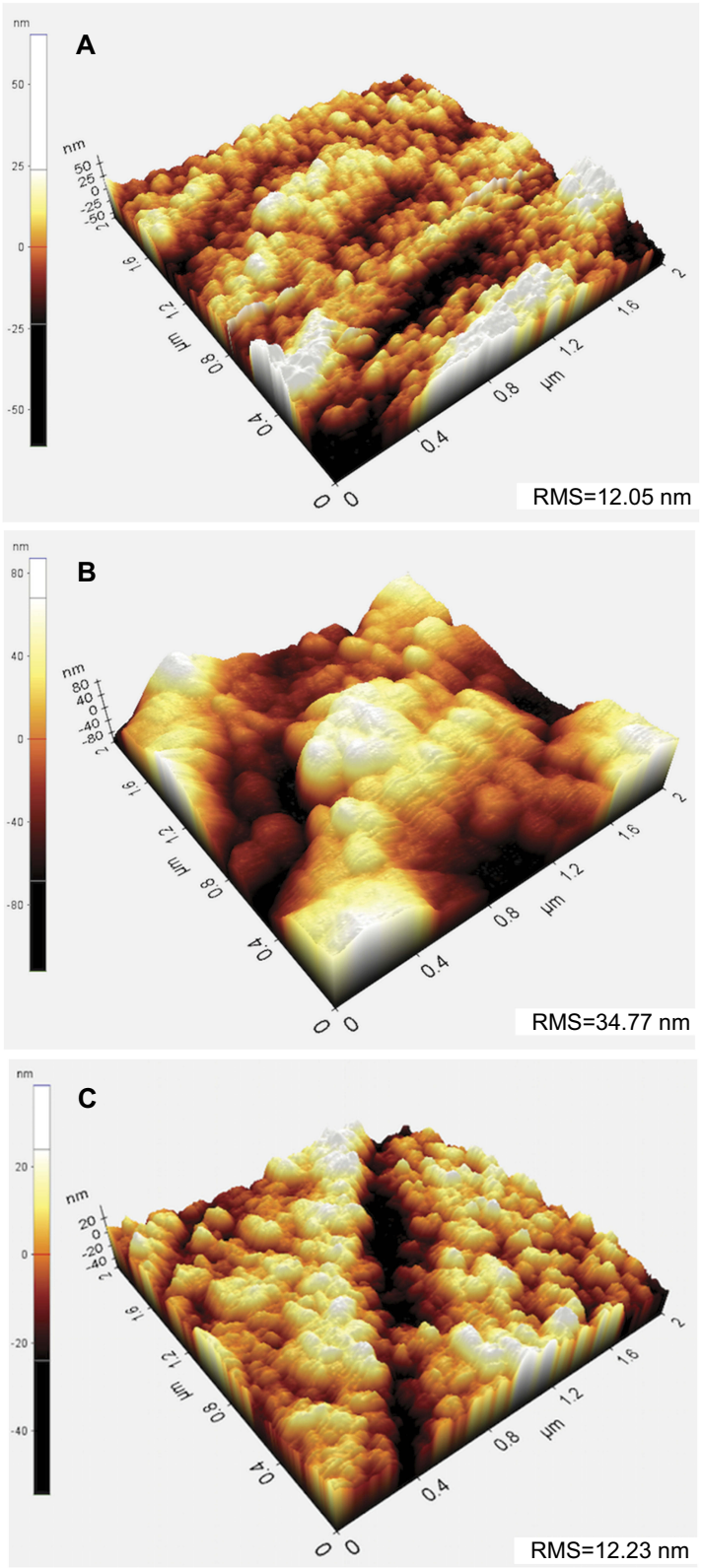

Figure 2 AFM images and RMS roughness of (**A**) Mg-Zn control, (**B**) Mg-Zn-TiO_2 (150°C), and (**C**) Mg-Zn-TiO_2 (200°C).
Abbreviations: AFM, atomic force microscopy; RMS, root mean square; Mg, magnesium; Zn, zinc; TiO_2, titanium dioxide.

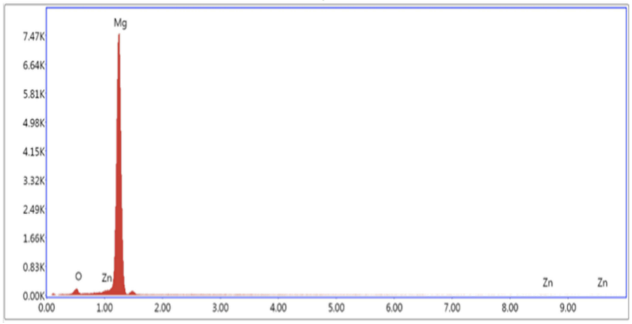

Figure 3 Energy-dispersive X-ray spectroscopy data results for the Mg-Zn alloy control.
Abbreviations: Mg, magnesium; Zn, zinc.

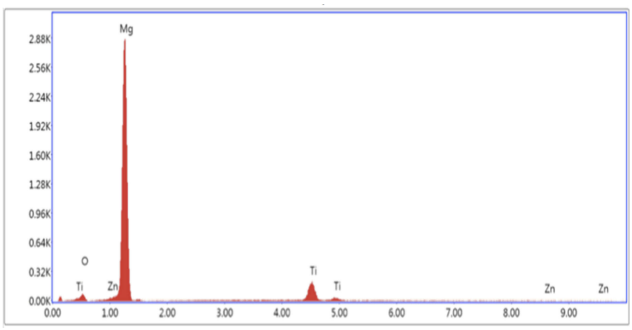

Figure 4 Energy-dispersive X-ray spectroscopy data results for Mg-Zn-TiO_2-150°C.
Abbreviations: Mg, magnesium; Zn, zinc; TiO_2, titanium dioxide.

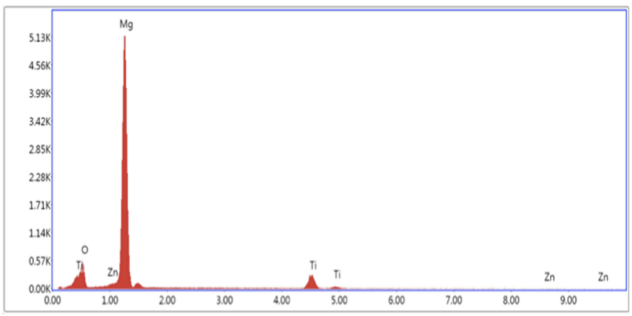

Figure 5 Energy-dispersive X-ray spectroscopy data results for Mg-Zn-TiO_2-200°C.
Abbreviations: Mg, magnesium; Zn, zinc; TiO_2, titanium dioxide.

density for Mg-Zn-TiO_2 (150°C) samples was enormously higher than those measured on Mg-Zn controls (Figure 11). However, Mg-Zn-TiO_2 (200°C) samples showed a much smaller increase in HCAEC density compared to controls.

Discussion

In this study, a well-established ALD coating technology with unique self-limiting and self-terminating reaction characteristics was used to chemically graft a TiO_2 thin coating with nanoscale thickness on Mg-Zn binary alloy stents. ALD

Table 1 Elemental Concentration Summary of Mg-Zn Alloy Samples Before and After ALD by Energy-Dispersive X-Ray Spectroscopy

Samples	Mg	Zn	Ti	O
Mg-Zn control	95.13	1.93	N/A	2.94
Mg-Zn-TiO_2 (150°C)	72.01	1.53	21.69	4.77
Mg-Zn-TiO_2 (200°C)	69.91	1.55	14.47	14.08

Abbreviations: Mg, magnesium; Zn, zinc; Ti, titanium; O, oxygen; TiO_2, titanium dioxide.

is a more controllable coating method compared to other coating techniques (such as CVD, IBAD, and PLD) for the deposition of uniform films with precise thickness. In addition, the surface morphology of the deposited TiO_2 films can be controlled by varying processing temperatures to achieve favorable crystallinity and surface structures.[41] Following the implantation of a material in the body, a series of biological events, involving protein adsorption and cell adhesion, can occur on the surface of implanted materials.[42] Since biomaterials are designed to function under physiological environments, surface chemistry and topography of the materials are particularly important for the advent of host responses and cell growth at the tissue–material interface.[43] Therefore, an ideal implant material should possess a biocompatible, non-toxic and tolerable surface for higher tissue growth. A Mg-Zn alloy is a conventional BVS material that interacts with the coronary artery lumen. Therefore, a Mg-Zn alloy was selected to be modified with an ALD treatment here.

Stenosis is caused by the deposition of excessive fat under the endothelium. While BVS can be implanted into the coronary artery through PCI, a balloon is used to expand the narrowed coronary artery several times in order to reshape the bloodstream. As a result, the diseased endothelium with excessive fat deposition beneath the vessel wall is widened by the balloon and the blocked bloodstream is opened up. During the PCI procedure, the sudden expansion and deployment of BVS can damage the endothelium monolayer consisting of endothelial cells. The endothelium is the fundamental regulator of vascular tone and thrombogenicity that separates bloodstream components such as platelets and the lumen wall.[44] In particular, limited growth of HCAECs can cause a delayed revascularization process as well as in-stent inflammation and restenosis.

In our results, with the SEM image morphological observation shown in Figure 1A–C, a 100 nm TiO_2 thin film can be clearly visualized compared with the untreated Mg-Zn

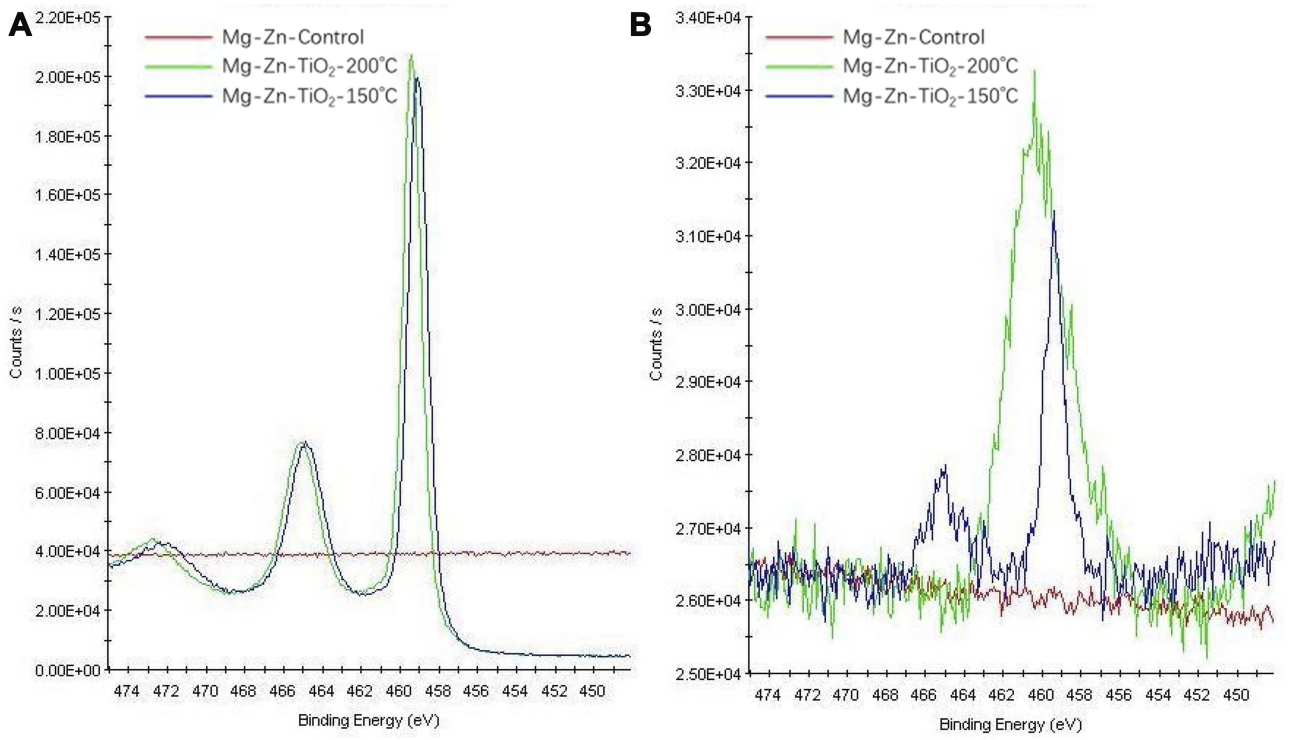

Figure 6 X-ray photoelectron spectroscopy graphs for a titanium scan of a Mg-Zn alloy control and Mg-Zn-TiO_2 coating at 150°C and 200°C: (**A**) without soaking in medium and (**B**) a 3-day soaking in medium.
Abbreviations: Mg, magnesium; Zn, zinc; TiO_2, titanium dioxide.

control. Intensive agglomeration with a raise in temperature was observed from 150 °C to 200 °C. Also, for the SEM images in Figure 1(C), a TiO_2 thin film coating at 200°C showed a higher distribution of visible crystallites compared to the ALD coating at 150°C (Figure 1B). The EDAX elemental composition analysis also indicated the existence of a TiO_2 thin film with increased elemental percentage of both Ti and O_2 compared to the control (Table 1). However, the different elemental percentage ratios of Ti to O for the ALD coating with the same thickness may be caused by the crystallite structure formed by the TiO_2 coating at 200°C. A TiO_2 nano-thin film coating was reported to have unstable properties at a coating temperature at 190°C.[28] By visualizing the 3D surface topography (Figure 2) of the Mg-Zn samples, a rougher surface can be observed after ALD treatment for TiO_2 coated at 150°C. However, the AFM RMS results did not show an increasing trend of surface roughness as the ALD operating temperature increased. ALD treatment at 200°C did not change the surface roughness of the substrate compared to controls. This might be caused by the different TiO_2 anatase crystallites formed on the surface which are different from the amorphous surface structure created at 150°C. XPS analysis also illustrated the degradation of Mg-Zn-TiO_2 (200°C) after being immersed in the cell culture medium for 3 days (Figure 3B). The absence of the secondary TiO_2 peak at 465eV in the XPS spectra indicated the degradation of the thin film. In contrast, the TiO_2 thin film coating of Mg-Zn-TiO_2 (150°C) remained stable after soaking in cell medium for 3 days. The different surface crystallinity of Mg-Zn-TiO_2 (200°C) can be identified with XRD analysis. As shown in the XRD patterns (Figure 4), a peak representing TiO_2 anatase appeared at $2\theta = 25.7°$, which was consistent as previously reported with the formation of anatase crystallites on the surface of the material when the TiO_2 thin film was deposited above 160°C.[45]

Furthermore, protein adsorption on the biomaterial surface is the initial event that occurs when the BVS is implanted. The amount of specific-absorbed proteins is associated with cell attachment since proteins can interact with cell membranes, and could protect surfaces from being colonized by bacteria.[46] The adsorbed protein layer can affect the interactions of cells with the surface and allow for downstream cellular activities such as cell spreading and proliferation.[47] The degree of hydrophilicity of biomaterial surfaces is one of the main factors that affect protein adsorption. Therefore, we measured the water contact angles to

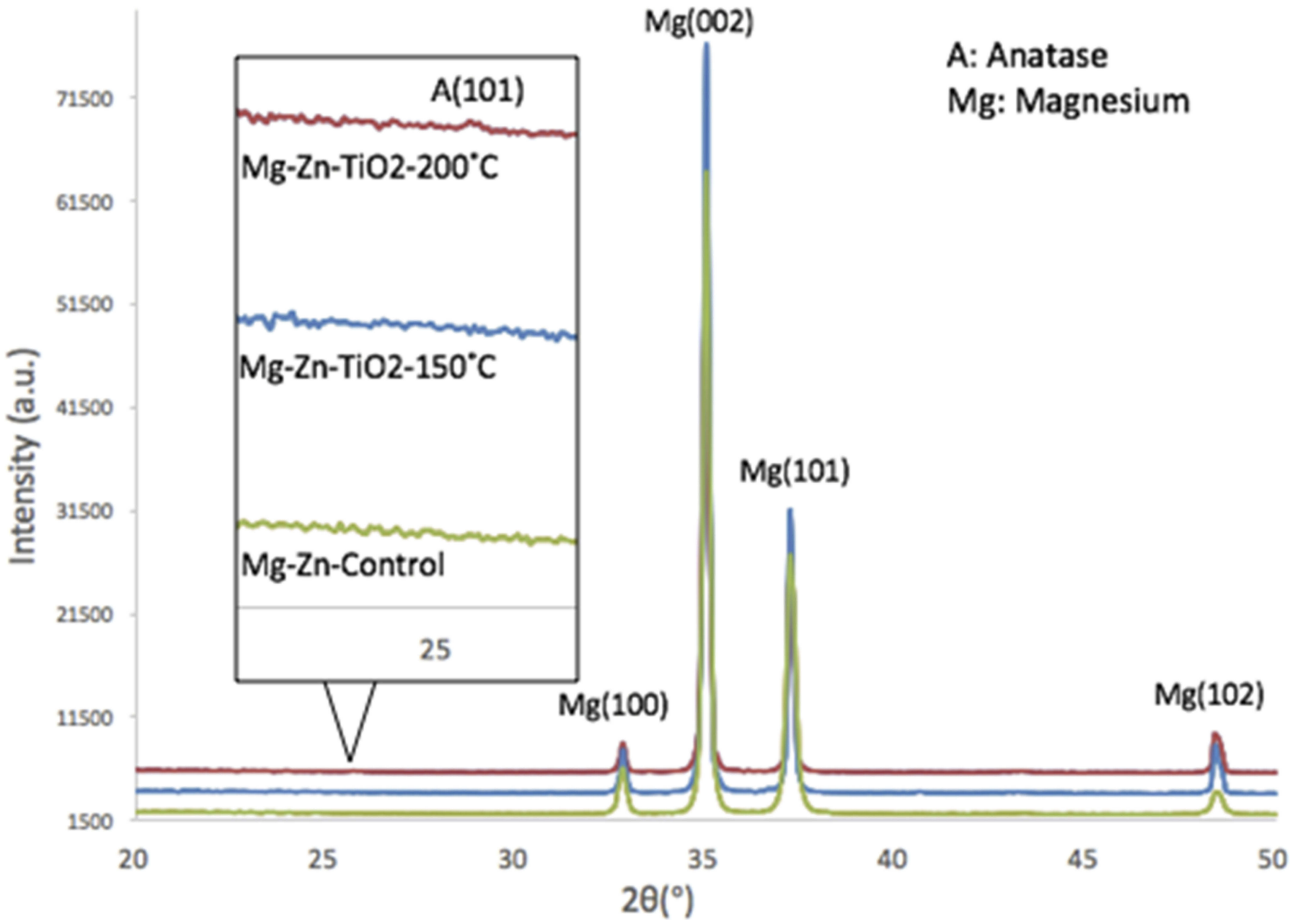

Figure 7 X-ray diffraction patterns of Mg-Zn alloy control and Mg-Zn-TiO_2 coating at 150°C and 200°C.
Abbreviations: Mg, magnesium; Zn, zinc; TiO_2, titanium dioxide.

evaluate the hydrophobicity of the Mg-Zn substrates with or without ALD treatment. The results showed that the ALD treatment caused increased water contact angles, and thus, higher hydrophobicity, in fact, values closer to the energy of proteins known to promote endothelial cell adhesion and growth (such as vitronectin and fibronectin). In addition, higher ALD operating temperatures resulted in an increase of total surface energy (Table 2), suggesting that the hydrophobicity of the ALD-treated substrates could be altered with operating temperature. Critically, other reports also showed that contact angles around 55 degrees possess the optimal surface energy to improve endothelial cell attachment.[48] In this protein adsorption study, we used BSA as a model protein. As Figure 9 shows, a TiO_2 nanoscale thin film grown on the Mg-Zn alloy substrates by ALD (operated at 150 °C or 200 °C) showed a slight increase in BSA protein adsorption, but not statistically; future studies should investigate this further as well as the adsorption of other proteins.

Next, we further analyzed HCAECs adhesion and proliferation on the Mg-Zn alloy substrates. The fluorescence micrographs (Figure 10) showed that HCAECs were able to attach on all the substrates in the first 4 hrs. The number of adherent cells on Mg-TiO_2-150°C substrates was significantly higher than those on the control and Mg-TiO_2-200°C substrates. Cells grown on Mg-TiO_2-150°C substrates also displayed greater cell spreading and cytoskeleton development. The Mg-TiO_2-200°C samples showed decreased cell numbers compared with the other two sample groups. However, after 7 days of cell culture, the binary alloy control and Mg-TiO_2-200°C substrates induced very low HCAEC viability in vitro (Figure 8), and no significant increase in cell density was observed after 14 days of cell culture. In contrast, the Mg-Zn-TiO_2 (150°C) samples resulted in a pronounced proliferation of HCAECs over 7 days of cell culture with a cell density at $1.5x10^5$ cells/cm^2. After 14 days of cell proliferation, HCAEC density grew even higher ($2.0x10^5$ cells/cm^2) presumably forming a desirable monolayer. On the other hand, Mg-Zn-

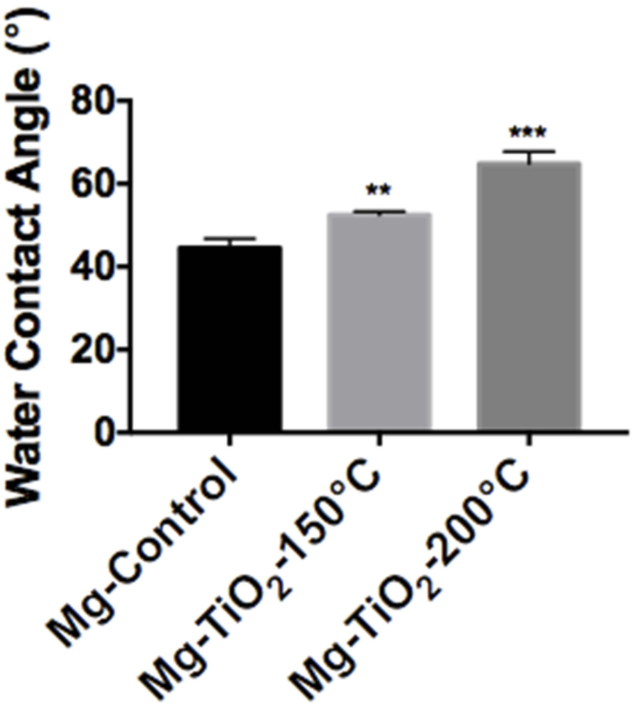

Figure 8 Water contact angle measurements on Mg-Zn alloy samples with different TiO_2 ALD coatings temperatures. Data represent mean ± standard deviation, N=3; **p<0.01; ***p<0.001 compared with control.
Abbreviations: Mg, magnesium; Zn, zinc; TiO_2, titanium dioxide.

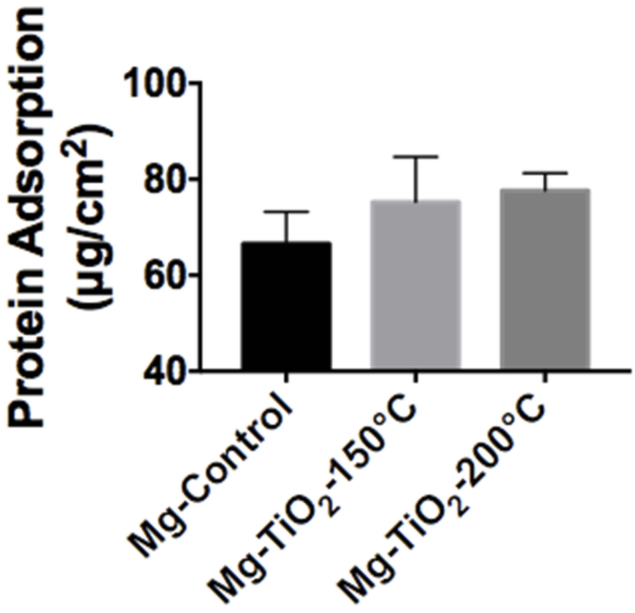

Figure 9 The amount of adsorbed bovine serum albumin on sample surfaces after 24 hrs of culture in a 0.01% BSA solution, N=3; data represents mean ± standard deviation.
Abbreviations: Mg, magnesium; Zn, zinc; TiO_2, titanium dioxide; BSA, bovine serum albumin.

TiO_2 (200°C) and Mg-Zn control samples did not promote cell growth. By looking at the results from the 4 hr cell adhesion fluorescent images (Figure 7A), although HCAECs adhered on the Mg-Zn control sample, the cellular cytoskeleton did not spread. Mg-Zn-TiO_2 (200°C) similarly induced a less spread cell morphology (Figure 7C).

We hypothesized that an ALD treatment with an operating temperature at 150 °C can improve the cytocompatibility of the Mg-Zn substrates to HCAECs. In contrast, although cells could attach on the untreated substrates, cell proliferation may have been inhibited by toxic substances generated by Mg degradation as a result of extended incubation time. During Mg degradation, one of the side products, OH^- ions, are generated. The release of OH^- ions may exhaust the physiological buffering system and cause further tissue necrosis which results in cell death or changes in cell activities due to alkalinization.[49] This could be the reason for the low HCAEC viability on the untreated Mg-Zn control. In addition, greater hydrophobicity of the Mg-Zn-TiO_2 (200°C) samples with a different surface structure compared with Mg-Zn-TiO_2 (150°C) can be unfavorable for cell growth, which showed a decreased in HCAECs density through 7–14 days of cell proliferation.

Table 2 Summary of Surface Wettability and Surface Energy of Mg-Zn Samples with Different TiO_2 Coatings

Samples	Surface Wettability (Contact Angle/°)	Surface Energy (mN/m)		
		γ_s^l	γ_s^p	γ_s^d
Mg-Zn Control	44.57 ± 0.038	44.66	28.67	15.98
Mg-Zn-TiO_2 (150°C)	52.50 ± 0.014	39.41	25.31	14.11
Mg-Zn-TiO_2 (200°C)	64.80 ± 0.038	30.96	19.88	11.08

Abbreviations: Mg, magnesium; Zn, zinc; TiO_2, titanium dioxide.

Even though the TiO_2 thin films coated on Mg-Zn alloys were slightly more hydrophobic than the untreated substrates, the Mg-Zn-TiO_2 (150°C) sample promoted cell adhesion and proliferation, indicating their potential to be a suitable BVS platform. On the other hand, Mg-Zn-TiO_2 (200°C) with the same TiO_2 thin film coating thickness (100 nm) but different surface morphologies were found unsuitable for stent applications since it was unfavorable for cell adhesion and proliferation.

As for future directions, long-term simulated body fluid (SBF) simulations to obtain relatively reliable implant functioning time period results in vitro would be necessary if the value meets the minimum revascularization requirement (5–6 months). In addition, ALD TiO_2 thin film coatings can be further optimized to find the best processing

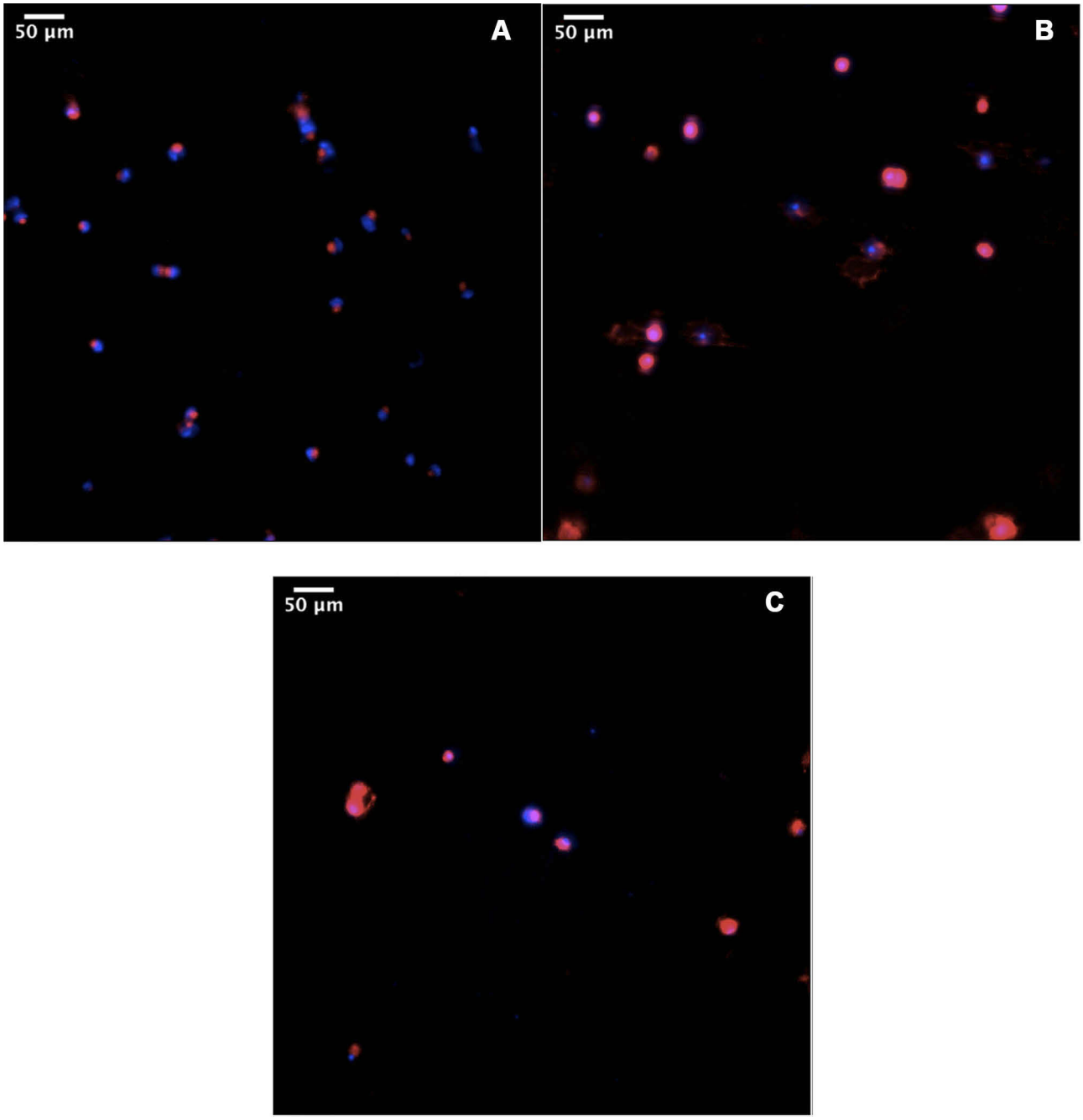

Figure 10 Fluorescent microscope image of (**A**) Mg-Zn control, (**B**) Mg-Zn-TiO_2 (150°C), (**C**) Mg-Zn-TiO_2 (200°C).
Abbreviations: Mg, magnesium; Zn, zinc; TiO_2, titanium dioxide.

temperature for promoting cell behavior. C-reactive protein (CRP) adsorption assays testing ALD coatings would be recommended since CRP is closely related to in-stent inflammation responses which results in in-stent restenosis.[50] Macrophages and foreign body giant cells should also be tested in vitro since macrophages and foreign body giant cells have been used as a marker for foreign body reactions.[7]

Of course, it is also recommended to conduct in vivo studies to further analyze the performance of this technology. The strut thickness of the BVS may result in frequent side-branch occlusions and result in periprocedural myocardial infarction. Early causes of BVS failure include scaffold dislodgement, acute recoil, and scaffold thrombosis.[51] The concept of the BVS is attractive. The short-term results here are encouraging according to previous reports, but long-term

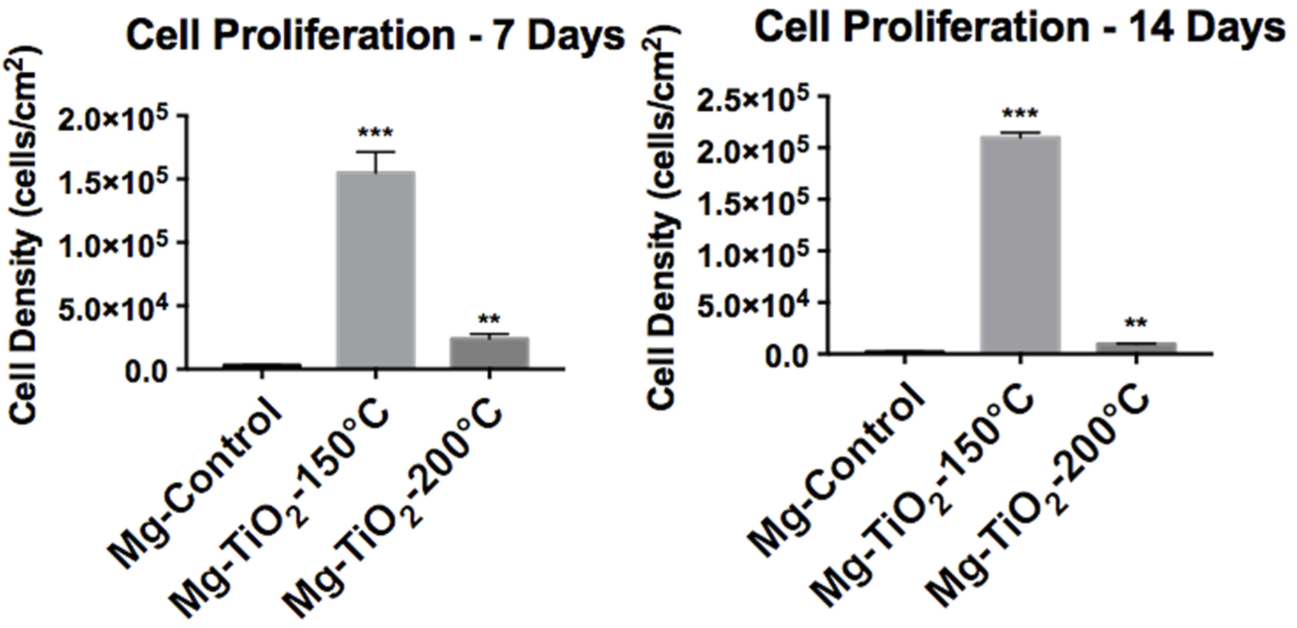

Figure 11 Human coronary endothelial cell proliferation on Mg-Zn alloy control and Mg-Zn-TiO_2 (150°C, 200°C) samples. Data represent mean ± standard deviation, N=3; **p<0.01 and ***p<0.001 compared with control.
Abbreviations: Mg, magnesium; Zn, zinc; TiO_2, titanium dioxide.

safety remains unknown. Therefore, more long-term clinical data will be required to determine whether these BVS can be used clinically.

Conclusion

The results of this study showed for the first time that using nano-thin film growth technology, ALD, to coat TiO_2 on Mg-Zn alloy stents (which serve as a BVS platform for treating blocked arteries), promoted endothelial cell adhesion and proliferation at ALD coating temperatures at 150°C. The TiO_2 nanoscale thin film acted as a protective barrier to prevent exposure of the underlying metal to immune cells in the bloodstream. Moreover, the protective TiO_2 layer has the potential to reduce the initial degradation rate of bare Mg-Zn alloys so that the biomaterial will not lose its functionality before the completion of the revascularization period (5–6 months). An ALD coating at 200°C did not show such positive outcomes with cell assays due to its unstable surface morphology and less than optimal surface energy, which did not match that of key proteins for mediating endothelial cell attachment. A well-designed fully bioresorbable implant material should promote endothelial cell growth without additional drug elution. As a result, ALD thin film coating technology has a strong potential to be applied to metallic coronary stents with optimized processing temperature control.

Acknowledgments

The authors would like to acknowledge the George J. Kostas Nano-scale Technology and Manufacturing Research Center at Northeastern University, and the Center for Nanoscale Systems, Harvard University, for providing the facilities for material characterization. Also, the authors would like to thank Catherina B. Garcia and Zelong Xie for performing XPS and XRD characterization. Lastly, the authors thank Northeastern University for funding.

Disclosure

The authors report no conflicts of interest in this work.

References

1. Zipes DP, Libby P, Bonow RO, Mann DL, Tomaselli GF. Braunwald's Heart Disease*: A Textbook of Cardiovascular Medicine*. Elsevier/Saunders; 2018.
2. Iqbal J, Gunn J, Serruys PW, et al. Coronary stents: historical development, current status and future directions. *Br Med Bull*. 2013;106(1):193–211. doi:10.1093/bmb/ldt009
3. Garg S, Serruys PW. Coronary stents current status. *J Am Coll Cardiol*. 2010;56(10):S1–S42. doi:10.1016/j.jacc.2010.06.007
4. Brie D, Penson P, Serban MC, et al. Bioresorbable scaffold – a magic bullet for the treatment of coronary artery disease? *Int J Cardiol*. 2016;215:47–59. doi:10.1016/j.ijcard.2016.04.027
5. Serruys P, Strauss BH, Beatt KJ, et al. Angiographic follow-up after placement of a self-expanding coronary-artery stent. *N Engl J Med*. 1991;324(1):13–17. doi:10.1056/NEJM199101033240103
6. Kereiakes DJ, Onuma Y, Serruys PW, et al. Bioresorbable vascular scaffolds for coronary revascularization. *Circulation*. 2016;134(2):168–182. doi:10.1161/CIRCULATIONAHA.116.021539

7. Kounis NG, Koniari I, Roumeliotis A, et al. Thrombotic responses to coronary stents, bioresorbable scaffolds and the kounis hypersensitivity-associated acute thrombotic syndrome. *J Thorac Dis*. 2017;9(4):1155–1164. doi:10.21037/jtd
8. Kounis NG, Zavras GM. Histamine-induced coronary artery spasm: the concept of allergic angina. *Br J Clin Pract*. 1991;45(2):121–128.
9. Kounis NG. Kounis syndrome: an update on epidemiology, pathogenesis, diagnosis and therapeutic management. *Clin Chem Lab Med*. 2016;54(10):1545–1559. doi:10.1515/cclm-2016-0010
10. Absorb bioresorbable vascular scaffold system. *Home*. Available from: www.vascular.abbott/us/products/coronary-intervention/absorb-bioresorbable-scaffold-dissolving-stent.html. Accessed December 11, 2019.
11. Azzalini L, L'Allier PL. Bioresorbable vascular scaffold thrombosis in an all-comer patient population: single-center experience. *J Invasive Cardiol*. 2015;27(2):85–92.
12. REal world advanced experience of BioResorbable ScaffolD by SMart Angioplasty Research Team (SMART REWARD) - full text view. *Full Text View - ClinicalTrials.gov*. Available from: clinicaltrials.gov/ct2/show/NCT02601404. Accessed December 11, 2019.
13. Yang J, Jao B, McNally AK, et al. In vivo quantitative and qualitative assessment of foreign body giant cell formation on biomaterials in mice deficient in natural killer lymphocyte subsets, mast cells, or the interleukin-4 receptor[alpha] and in severe combined immunodeficient mice. *J Biomed Mater Res Part A*. 2014;102(6):2017–2023. doi:10.1002/jbm.a.35152
14. Lendlein A, Langer R. Biodegradable, elastic shape-memory polymers for potential biomedical applications. *Science*. 2002;296(5573):1673–1676. doi:10.1126/science.1066102
15. Yoon SJ, Kim SH, Ha HJ, et al. Reduction of inflammatory reaction of poly(D,L-lactic-co-glycolic acid) using demineralized bone particles. *Tissue Eng Part A*. 2008;14(4):539–547. doi:10.1089/tea.2007.0129
16. Ji W, Yang F, Seyednejad H, et al. Biocompatibility and degradation characteristics of PLGA-based electrospun nanofibrous scaffolds with nanoapatite incorporation. *Biomaterials*. 2012;33(28):6604–6614. doi:10.1016/j.biomaterials.2012.06.018
17. Prove letter of absorb GT1™ Bioresorbable Vascular Scaffold (BVS) system. Available from: http://www.accessdata.fda.gov/cdrh_docs/pdf15/P150023a.pdf. Accessed December 11, 2019.
18. Song G, Song S. A possible biodegradable magnesium implant material. *Adv Eng Mater*. 2007;9(4):298–302. doi:10.1002/(ISSN)1527-2648
19. Li N, Zheng Y. Novel magnesium alloys developed for biomedical application: a review. *J Mater Sci Technol*. 2013;29(6):489–502. doi:10.1016/j.jmst.2013.02.005
20. Tapiero H, Tew KD. Trace elements in human physiology and pathology: zinc and metallothioneins. *Biomed Pharmacother*. 2003;57(9):399–411. doi:10.1016/S0753-3322(03)00081-7
21. Bowen PK, Drelich J, Goldman J, et al. Zinc exhibits ideal physiological corrosion behavior for bioabsorbable stents. *Adv Mater*. 2013;25(18):2577–2582. doi:10.1002/adma.201300226
22. Zhang S, Li J, Song Y, et al. In vitro degradation, hemolysis and MC3T3-E1 cell adhesion of biodegradable Mg–zn alloy. *Mater Sci Eng C*. 2009;29(6):1907–1912. doi:10.1016/j.msec.2009.03.001
23. Zhang S, Zhang X, Zhao C, et al. Research on an Mg–Zn alloy as a degradable biomaterial. *Acta Biomater*. 2010;6(2):626–640. doi:10.1016/j.actbio.2009.06.028
24. Kirkland NT. Magnesium biomaterials: past, present and future. *Corros Eng Sci Technol*. 2012;47(5):322–328. doi:10.1179/1743278212Y.0000000034
25. Koch CF, Johnson S, Kumar D, et al. Pulsed laser deposition of hydroxyapatite thin films. *Mater Sci Eng C-Biomimetic and Supramolecular Syst*. 2007;27(3):484–494. doi:10.1016/j.msec.2006.05.025
26. Yang JX, Jiao YP, Cui FZ, et al. Modification of degradation behavior of magnesium alloy by IBAD coating of calcium phosphate. *Surf Coat Technol*. 2008;202(22):5733–5736. doi:10.1016/j.surfcoat.2008.06.035
27. Wank JR, George SM, Weimer AW, et al. Coating fine nickel particles with Al_2O_3 utilizing an Atomic Layer Deposition-Fluidized Bed Reactor (ALD–FBR. *J Am Ceram Soc*. 2004;87(4):762–765. doi:10.1111/jace.2004.87.issue-4
28. Liu L, Bhatia R, Webster T. et al. Atomic layer deposition of Nano-TiO_2 thin films with enhanced biocompatibility and antimicrobial activity for orthopedic implants. *Int J Nanomedicine*. 2017. 8711–8723. doi:10.2147/IJN
29. Skocaj M, Filipic M, Petkovic J, et al. Titanium dioxide in our everyday life; is it safe? *Radiol Oncol*. 2011;45(4):227–247. doi:10.2478/v10019-011-0037-0
30. FDA [Internet]. Food and drugs chapter I, Listing of color additives exempt from certification. Federal Register 21CFR73, US Rockville, MD; 2010 [cited October 2011, 14]. Available from: http://www.accessdata.fda.gov/scripts/cdrh/cfdocs/cfcfr/CFRSearch.cfm?CFRPart=73&showFR=1. Accessed December 11, 2019.
31. Rowe RC, Sheskey PJ, Weller PJ. *Handbook of Pharmaceutical Excipients*. Fourth ed. London: Pharmaceutical Press; The American Pharmaceutical Association; 2003.
32. Shen GX, Chen YC, Lin L, et al. Study on a hydrophobic nano-TiO2 coating and its properties for corrosion protection of metals. *Electrochim Acta*. 2005;50(25):5083–5089. doi:10.1016/j.electacta.2005.04.048
33. Basiaga M, Walke W, Staszuk M, et al. Influence of ALD process parameters on the physical and chemical properties of the surface of vascular stents. *Arch Civ and Mech Eng*. 2017;17(1):32–42. doi:10.1016/j.acme.2016.08.001
34. Onn TM, Küngas R, Fornasiero P, et al. Atomic layer deposition on porous materials: problems with conventional approaches to catalyst and fuel cell electrode preparation. *Inorganics*. 2018;6(1):34. doi:10.3390/inorganics6010034
35. Owens DK, Wendt RC. Estimation of the surface free energy of polymers. *J Appl Polym Sci*. 1969;13(8):1741–1747. doi:10.1002/app.1969.070130815
36. Aarik J, Aidla A, Uustare T, Sammelselg V. Morphology and structure of TiO2 thin films grown by atomic layer deposition. *J Cryst Growth*. 1995;148(3):268–275. doi:10.1016/0022-0248(94)00874-4
37. Jenei, Jenei P, Gubicza J, et al. X-ray diffraction study on the microstructure of a Mg–zn–Y alloy consolidated by high-pressure torsion. *J Alloys Compd*. 2012;539(C):32–35. doi:10.1016/j.jallcom.2012.05.100
38. Liu K, Cao M, Fujishima A, et al. Bio-inspired titanium dioxide materials with special wettability and their applications. *Chem Rev*. 2014;114(19):10044–10094. doi:10.1021/cr4006796
39. Xu LC, Siedlecki CA. Effects of surface wettability and contact time on protein adhesion to biomaterial surfaces. *Biomaterials*. 2007;28(22):3273–3283. doi:10.1016/j.biomaterials.2007.03.032
40. Brutsaert DL, Fransen P, Andries LJ, De Keulenaer GW, Sys SU. Cardiac endothelium and myocardial function. *Cardiovasc Res*. 1998;38(2):281–290. doi:10.1016/S0008-6363(98)00044-3
41. Miikkulainen V, Leskelä M, Ritala M, Puurunen RL. Crystallinity of inorganic films grown by atomic layer deposition: overview and general trends. *J Appl Phys*. 2013;113(2):2.
42. Rolfe B, Mooney J, Zhang B, et al. The fibrotic response to implanted biomaterials: implications for tissue engineering. *Regener Med Tissue Eng - Cells Biomater*. 2011. doi:10.5772/21790
43. Chen H, Yuan L, Song W, Wu Z, Li D. Biocompatible polymer materials: role of protein–surface interactions. *Prog Polym Sci*. 2008;33(11):1059–1087. doi:10.1016/j.progpolymsci.2008.07.006
44. Sumpio, Sumpio BE, Timothy Riley J, et al. Cells in focus: endothelial cell. *Int J Biochem Cell Biol*. 2002;34(12):1508–1512. doi:10.1016/S1357-2725(02)00075-4
45. Luka G, Witkowski BS, Wachnicki L, et al. Kinetics of anatase phase formation in TiO2 films during atomic layer deposition and post-deposition annealing. *CrystEngComm*. 2013;15(46):9949–9954. doi:10.1039/c3ce40893k

46. Felgueiras HP, Antunes JC, Martins MCL, Barbosa MA. 1 - Fundamentals of protein and cell interactions in biomaterials. In: Mário A, Barbosa M, Martins CL, editors. *Peptides and Proteins as Biomaterials for Tissue Regeneration and Repair*. Woodhead Publishing; 2018:1–27.
47. Anderson J. Biological responses to materials. *Annu Rev Mater Res*. 2001;31:81–110. doi:10.1146/annurev.matsci.31.1.81
48. Raimondo T, Puckett S, Webster TJ, et al. Greater osteoblast and endothelial cell adhesion on nanostructured polyethylene and titanium. *Int J Nanomedicine*. 2010;5(1):647–652. doi:10.2147/IJN.S13047
49. Seitz J-M, Eifler R, Bach F-W, et al. Magnesium degradation products: effects on tissue and human metabolism. *J Biomed Mater Res Part A*. 2014;102(10):3744–3753. doi:10.1002/jbm.a.35023
50. Li J-J, Ren Y, Chen K-J, et al. Impact of C-reactive protein on in-stent restenosis: a meta-analysis. *Tex Heart Inst J*. 2010;37 (1):49–57.
51. Tan HC, Ananthakrishna R. A review of bioresorbable scaffolds: hype or hope? *Singapore Med J*. 2017;58(9):512–515. doi:10.11622/smedj.201617